Journal of Fluids and Structures 65 (2016) 447–454

Contents lists available at ScienceDirect

Journal of Fluids and Structures

journal homepage: www.elsevier.com/locate/jfs

Coupling between a flag and a spring-mass oscillator

Emmanuel Virot [a,*], Xavier Amandolese [a,b], Pascal Hémon [a]

[a] Laboratoire d'Hydrodynamique (LadHyX), CNRS UMR 7646, École Polytechnique – 91128 Palaiseau, France
[b] Conservatoire National des Arts et Métiers – 75003 Paris, France

ARTICLE INFO

Article history:
Received 21 September 2015
Received in revised form
8 June 2016
Accepted 13 June 2016

Keywords:
Flag flutter
Lock-in
Fluid–structure interaction
Energy harvesting

ABSTRACT

In the context of energy harvesting we address the coupling between a flexible flag and its flagpole equipped so that it constitutes a spring-mass oscillator. An extensive set of experiments is carried out in wind tunnel for various flag and oscillator parameters. Results are analyzed in terms of frequency and amplitude of rotation of the flagpole. We report numerous configurations of coupling by frequency lock-in leading to resonance conditions. In the case of strong coupling, high amplitudes of rotation of the flagpole are reported, up to 75° peak-to-peak, over a large range of wind velocities. We also propose to characterize the strength of the coupling with a dimensionless rigidity $\tilde{B}$, which can be considered as the ratio of the flag bending rigidity to the stiffness of the oscillator.

1. Introduction

Harvesting energy from flapping flags is an idea that has been intensively considered during the last decade. Two mechanisms are generally proposed for the excitation of the flag: either an external forcing by an unsteady flow, such as the wake of a bluff body (Allen and Smits, 2001; Taylor et al., 2001), or an intrinsic forcing by a steady flow destabilizing the flag by flutter (Tang et al., 2009). Two technical strategies for harvesting electric energy have also been described in previous works, either distributed or localised. On the one hand, the deformation of the flag can be used, for instance by covering the flag surface with piezoelectric patches, as in the recent experimental and numerical studies by Doaré and Michelin (2011), Dunnmon et al. (2011), Giacomello and Porfiri (2011), Singh et al. (2012), Akcabay and Young (2012), Michelin and Doaré (2013), and Xia et al. (2015). On the other hand, the displacement of the flag can be used, then taking advantage of electromagnetic induction or triboelectricity as in the recent experimental and numerical studies by Gibbs et al. (2012), Stone et al. (2013), Howell and Lucey (2014), and Bae et al. (2014).

A key point is that energy transfers are favoured in the situation of resonance. More precisely, it has been shown numerically that there is a strong increase in the efficiency of the harvesting in the presence of a frequency lock-in, in the context of the coupling between a piezoelectric flag and an electrical oscillator (resistance-inductance) studied by Xia et al. (2015). Moreover, in the context of vortex-induced vibrations, the frequency lock-in between the wake vortices and a cylinder-oscillator is essential (Khalak and Williamson, 1999; Williamson and Govardhan, 2004) and is already concretely used for harvesting energy from water currents (see Bernitsas et al., 2008). By comparison with systems based on flapping flags, a wake of vortex can be seen as the analogue of a flag. Both exert a periodic forcing on the oscillator, which can be significantly enhanced by the oscillator motion in the lock-in region.

In this paper, we focus on the intrinsic flutter instability of flags and we trigger frequency lock-in conditions between flapping flags and oscillating flagpoles, while varying the parameters of the flag and oscillator. Results are analyzed in terms of frequency and amplitude of rotation of the flagpole.

* Corresponding author.
E-mail address: emmanuel.virot@polytechnique.edu (E. Virot).

http://dx.doi.org/10.1016/j.jfluidstructs.2016.06.014
0889-9746/

2. Experiments

2.1. Experimental set-up

An Eiffel-type wind tunnel is used with wind velocities ranging from 3 to 20 m s^{-1} at a low turbulence level (0.4% over this velocity range). The wind tunnel has a rectangular test-section: width $\times$ height=260 mm $\times$ 240 mm. The flag is clamped inside of a flagpole of thickness 4 mm and height 140 mm. In our experiments, the Reynolds number based on the flag length (L) falls in the range $\mathrm{Re}_L = 1 \times 10^4 - 4 \times 10^5$.

The flagpole is not clamped in the wind tunnel. Rather, it is guided by two ball bearings, Fig. 1, making it free to rotate. An inertia bar and a set of linear springs are attached to the flagpole to modelize an elementary spring-mass oscillator.

The instantaneous amplitude of rotation of the flagpole is characterized by the rotation angle $\theta(t)$ between the inertia bar and the normal to the wind, Fig. 1(a). Since the flag is clamped to a rigid flagpole, the angle $\theta(t)$ is also the rotation angle of the leading edge of the flag. It is measured with a laser sensor recording 1024 acquisitions per second with an error lower than 1% in the range of angle from $-60°$ to $60°$. In this paper, the fluctuations of $\theta(t)$ are reported with the standard deviation $\sigma_\theta = \sqrt{\langle\theta^2\rangle - \langle\theta\rangle^2}$. The acquisition duration is 24 s, which is sufficient to record more that 100 flapping periods. Concerning the frequency analysis, noise is reduced by treating independently blocks of 8 s (with an overlap: 50%); the resulting frequency resolution is then 1/8 Hz.

2.2. Characteristics of the flag and spring-mass oscillator

The flapping frequency of flags must be sufficiently low to be coupled with the (low frequency) spring-mass oscillators, whose natural frequency can be varied between 1 Hz and 20 Hz. We used paper sheets (120 g m^{-2}, thickness d=153 μm) and steel sheets (thickness d=54, 77 or 103 μm). The mass densities of these sheets are respectively ρ_s = 790, 7290, 7620 and 7680 kg m^{-3}. The width of the flags is unchanged (H=100 mm), while the flag length is varied in the range L=60–300 mm. The size of the flags is chosen to limit blockage effect in the wind tunnel.

We have used two inertia bars, depending on the natural frequency needed: a thick aluminium bar and a thin carbon fiber bar. The moment of inertia J_{osc} of the system with the aluminium bar is 1.7×10^{-4} kg m^2, whereas it is 9.2×10^{-5} kg m^2 with the carbon fiber bar. In practice, the carbon fiber bar is quite unique to be both rigid and light (Ashby, 2000). Indeed, we pay a particular attention to the fact that a flexible inertia bar could interact with the flag. Here the bending rigidity of the bar is always 100 times larger than the stiffness of springs. If the natural frequency of the oscillator needs to be precisely adjusted, then additional masses may be placed along the inertia bar, allowing a variation of the inertia moment J_{osc} between 9.2×10^{-5} kg m^2 and 8.4×10^{-4} kg m^2.

We used linear spring with stiffness in the range 0.05–0.28 N mm^{-1}, leading to stiffness in rotation varying in the range C_{osc} = 0.28–2.3 N m rad^{-1}. For keeping the symmetry of the system, a particular attention is devoted to place identical springs in parallel, at the same distance from the axis of rotation.

The mechanical oscillator attached to the flagpole is irremediably damped. After a small perturbation of the system without flag, the exponential decrease of the rotation angle that we observed suggests that the damping is essentially viscous (Landau and Lifshitz, 1976, p. 75). The damping is therefore expressed by a dimensionless damping ratio ζ^*_{osc} (Landau

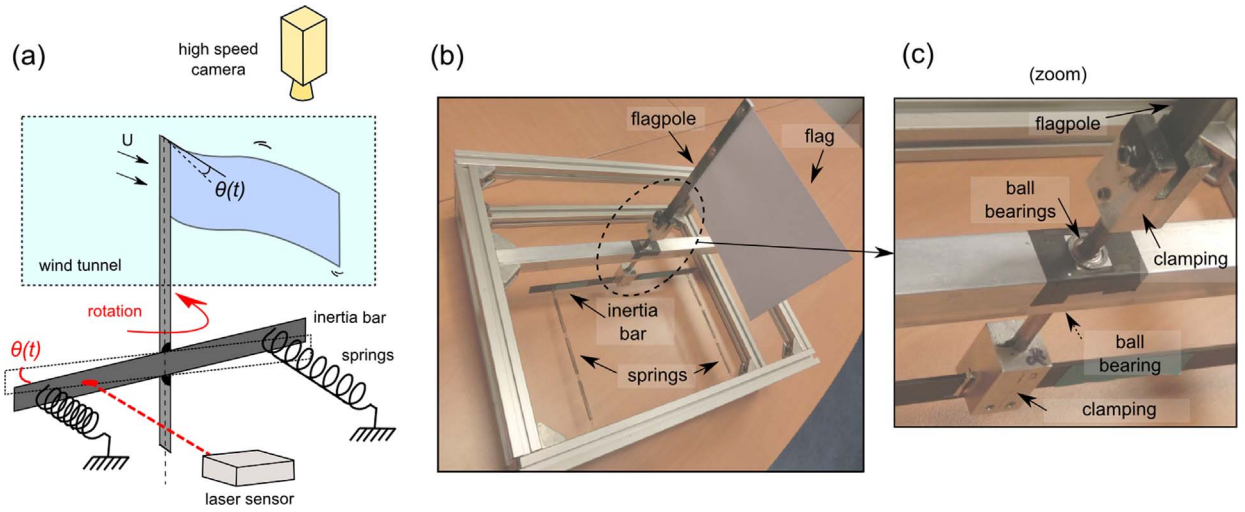

Fig. 1. Experimental set-up. (a) Schematic representation of the experiment. The flagpole is attached to a spring-mass oscillator, which is out of wind-tunnel. A laser sensor measures the angle of rotation θ of the rotating inertia bar fixed to the flagpole. (b,c) Photographs of the experimental set-up (here the whole system is out of wind-tunnel), where it can be seen that the flagpole is guided by ball bearings.

and Lifshitz, 1976), which is measured by adjusting a law $-\log(\theta)/\omega_{osc} \sim \zeta^*_{osc} t$ on the envelope of the temporal decrease of an impulse response. In this expression, the natural pulsation is defined classically: $\omega_{osc} = \sqrt{C_{osc}/J_{osc}} = 2\pi f_{osc}$.

Five independent free decay tests have been systematically carried out for each set of parameters of the oscillator. Results have shown that the damping ratio is constant $\zeta^*_{osc} \simeq 0.014$ in our experiments, except for the system of Section 2.3 where $\zeta^*_{osc} \simeq 0.005$.

2.3. A concrete example of frequency lock-in with a paper flag

Let us illustrate the "frequency lock-in" between a flag and an oscillator with a first concrete example. Tests have been done with a paper flag (120 g m^{-2}) of length $L=286$ mm and width $H=100$ mm.

In a clamped flagpole configuration, the flapping frequency evolution is shown in Fig. 2(a) as a function of the wind velocity, where we report the power spectral densities of the flapping moment measured in Virot et al. (2013). The wind velocity is kept constant about three minutes before the following increase. A dark color means a dominant frequency. The flapping frequency of the flag with a clamped flagpole increases almost linearly (from 10 Hz to 20 Hz) with the wind velocity.

In a coupled flagpole situation, with a flagpole-oscillator of natural frequency $f_{osc} \simeq 13.9$ Hz we then expect a resonance for a wind velocity $U=8.6$ m s^{-1}. Measurements of $\theta(t)$ have been done for wind velocity U in the range 5.0–11.0 m s^{-1}, with increments of 0.3 m s^{-1}. The striking effect of the coupling is reported in Fig. 2(b), where we observe the power spectral densities of $\theta(t)$. Between $U=6$ m s^{-1} and $U=8$ m s^{-1}, the oscillation frequency of the flagpole is almost identical to the flapping frequency of the same flag with a clamped flagpole, Fig. 2(a). Nevertheless, in the range of wind velocity $U=8$–9 m s^{-1}, the oscillation frequency of the flagpole deviates and remains locked with the natural frequency of the oscillator ($f_{osc} = 13.9$ Hz). Above $U=9$ m s^{-1}, we observe a strong modification of the dominant frequency, which switches to the typical flapping frequency of a clamped flag. This evolution bear some resemblances with the one recently observed for forced vibrations of flags in soap films (Jia et al., 2015). In Fig. 2, it seems that the critical wind velocity of flutter is lower in the case of the coupled flagpole. A more rigorous estimation of this effect would require further investigations.

The evolution of the standard deviation of the angle of rotation of the flagpole is shown in Fig. 3(a) as a function of the wind velocity. The measurements obtained with an increasing wind velocity are superimposed with the ones obtained with a decreasing wind velocity. One can observe a bent-over resonance curve for which the maximum peak-to-peak angle of rotation is close to 10°. However, if we draw the resonance curve as a function of the flapping frequency, Fig. 3(b), we obtain a classical linear resonance curve. It suggests that both the bent-over and hysteretic behaviour can be explained by the frequency lock-in, without any other retroaction of the oscillator on the dynamics of the flag. One can call this first configuration a "light coupling".

2.4. A concrete example of reproducibility with a steel flag

We choose for this second concrete example a more rigid flag and a less stiff spring-mass oscillator (by adding springs in series). The flag is made of steel, with a thickness $d=54$ μm, a length $L=150$ mm and a width $H=100$ mm. The spring-mass oscillator has a natural frequency $f_{osc} = 8.2$ Hz (with $C_{osc} = 0.28$ N m rad^{-1}, $J_{osc} = 1.0 \times 10^{-4}$ kg m^2 and $\zeta^*_{osc} = 0.014$). In order to

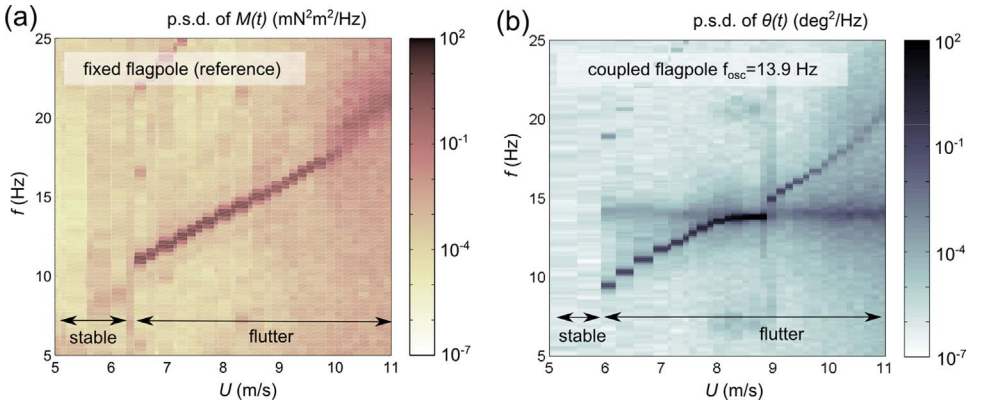

Fig. 2. Detection of the frequency lock-in by using power spectral densities reported vertically with a logarithmic colorbar (case of a paper flag). (a) Power spectral densities of the flapping moment of a flag with clamped flagpole (our reference case). We observe a dominant frequency, which increases linearly with wind velocity U. (b) Power spectral densities of $\theta(t)$, in the case of a coupling flag-oscillator. The natural frequency of the oscillator $f_{osc} \simeq 13.9$ Hz is visible in spectra. More particularly, an area of frequency lock-in is visible between $U=8$ m s^{-1} and $U=9$ m s^{-1}, where the flagpole oscillations are more intense (darker) and are even "locked" with the natural frequency f_{osc}. (For interpretation of the references to color in this figure caption, the reader is referred to the web version of this paper.)

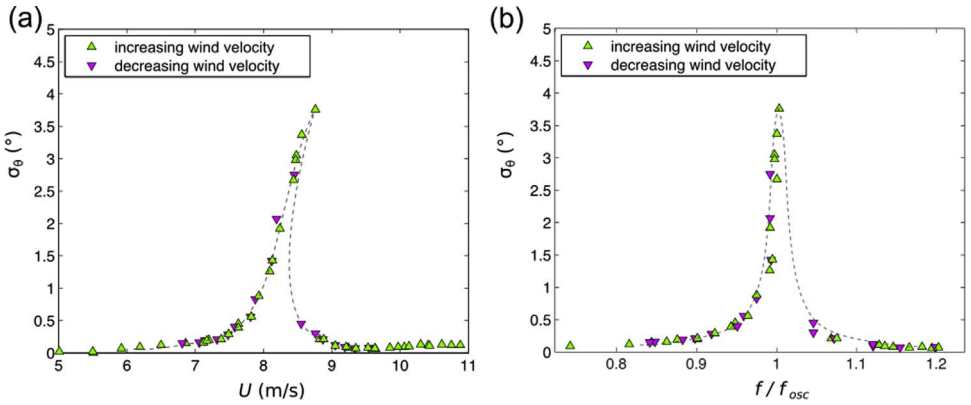

Fig. 3. Evolution of the fluctuations of $\theta(t)$, characterized by the standard deviation σ_θ (case of a paper flag). For each datapoint at a precise wind velocity, we wait about three minutes before recording, in order to not be affected by any transient signal. (a) We can think of a bent-over resonance curve when it is plotted as a function of the wind velocity. (b) Nevertheless, we observe a classical resonance curve as a function of the flapping frequency of the flag. The dotted lines are guides for the eyes.

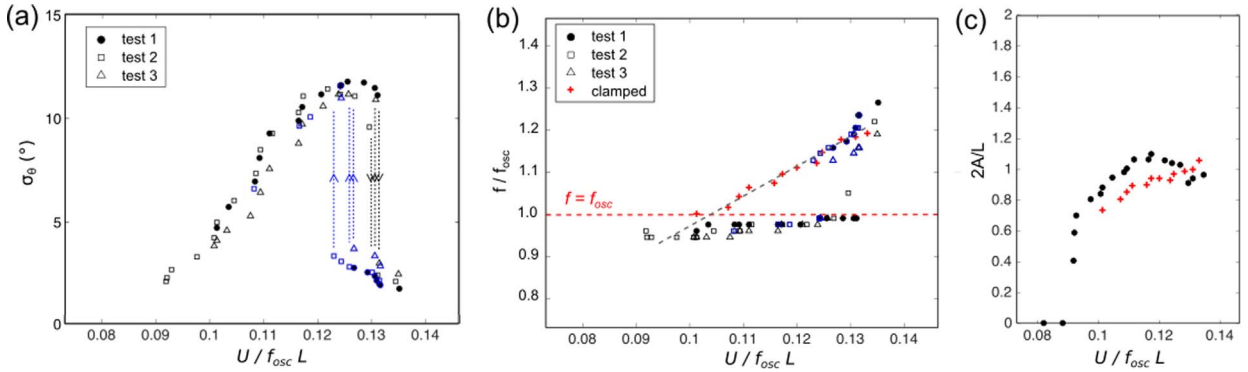

Fig. 4. Analysis of reproducibility (case of a steel flag). Values obtained by gradually increasing the wind velocity are superimposed with values obtained by gradually decreasing the wind velocity (blue color) and "test 1", "test 2", "test 3" denote the independent reproducibility tests made under the same experimental conditions. (a) Evolution of the standard deviation σ_θ of the angle of rotation of the flagpole as a function of the reduced wind velocity. (b) Dominant frequency of the flagpole oscillation. The natural frequency of the oscillator is indicated by the dotted horizontal line (f_{osc} = 8.2 Hz). The expected trend of the flapping frequency without lock-in is suggested by the gray dotted line, supported by experimental data measured at decreasing wind velocity (crosses). (c) Evolution of the amplitude peak-to-peak of the trailing edge of the flag in the coupled configuration (circles) and clamped (crosses), normalized by the flag length L. (For interpretation of the references to color in this figure caption, the reader is referred to the web version of this paper.)

assess the reproducibility of the "frequency lock-in", we perform three tests in the same conditions (same flag properties, same oscillator). Results are reported under a normalized form, introducing a reduced velocity, $U/f_{osc}L$, a relative frequency, f/f_{osc}, and a relative amplitude of the flag dynamics, $2A/L$, where $2A$ is the peak-to-peak amplitude of the trailing edge of the flag.

In Fig. 4(a), we report the successive measurements of the standard deviation σ_θ of the angle of flagpole rotation. The measurements obtained with an increasing wind velocity are superimposed with the ones obtained with a decreasing wind velocity in order to highlight the hysteresis phenomenon. We report the corresponding dominant frequencies in Fig. 4(b). We observe that the frequency lock-in phenomenon takes place over a large range of wind velocities U=5.1–7.2 m s^{-1} ($U/f_{osc}L$ = 0.09 – 0.13).

An identical value of the maximum of σ_θ is systematically found ($\simeq$11.2° with an error 4%). The extension of the frequency lock-in (in terms of wind velocities) is conserved as well. However, the critical wind velocity required to flutter is variable (difference: 10%). The measurements in Fig. 4(b) also suggest that the coupled configuration is more unstable to flutter than the clamped one, and from Fig. 4(c) it seems that the flag dynamics can be amplified during the frequency lock-in. Nevertheless, more detailed studies about these specific points would be necessary to confirms the trends.

Finally, when we compare the first example (flag made of paper, f_{osc} = 13.9 Hz) to the second example (flag made of steel, f_{osc} = 8.2 Hz), we clearly see that the maximal angle of rotation strongly vary (here from σ_θ^{max} = 3.8° to 11.2° in terms of standard deviations) when the parameters of the flag and oscillator are modified. In the following, we thus study quantitatively the influence of each parameter of the coupling.

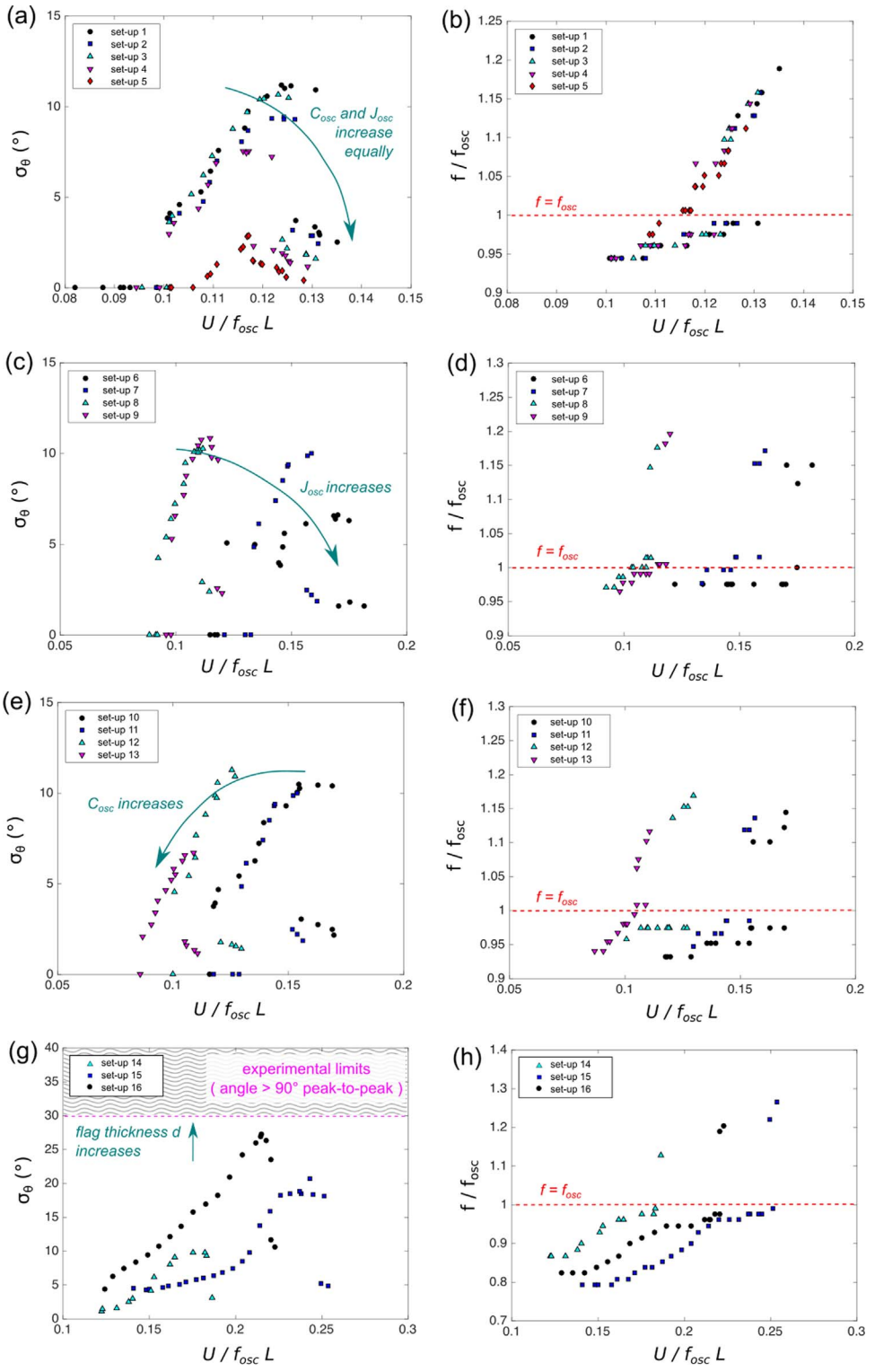

Fig. 5. Amplitude and frequency of the rotation of the flagpole for several parameters of coupling. The natural frequency of the oscillator is adjusted to be very slightly above the flapping frequency of the flag at the threshold of flutter instability. Values obtained by gradually increasing the wind velocity are superimposed with values obtained by gradually decreasing the wind velocity. (a,b) With variations of C_{osc} and J_{osc} (in the same proportions). (c,d) With variations of J_{osc} and L. (e,f) With variations of C_{osc} and L. (g,h) With variations of d and L.

3. Frequency lock-in at the threshold of instability

We perform experiments at the threshold of flutter instability in order to characterize the role of the stiffness and inertia of the oscillator along with the flag parameters. We adjust the natural frequency of the flagpole-oscillator around the critical flutter frequency of the clamped flag (at the lowest wind velocity where flutter instability can be observed). Note that this is an arbitrary choice, and that the natural frequency of the flagpole-oscillator could also be set at much larger values than the critical flutter frequency of the clamped flag, but with a risk of loss of periodicity at high wind velocities.

3.1. Results

We start by making a series of experiments, increasing equally C_{osc} and J_{osc} for a fixed value of the frequency f_{osc} close to 8.4 Hz (Fig. 5(a,b)). For each configuration, frequency lock-in is set close to the threshold of flutter instability of the flag. The threshold of flutter is estimated in the situation of a clamped flag during preliminary experiments, and we denote by $f_c^{clamped}$ the flapping frequency of the flag at the lowest wind velocity allowing to sustain the flutter instability (since flutter is subcritical, this value is obtained by decreasing the wind velocity). The parameters of the flags and oscillators are reported in Table 1. In Fig. 5(a), we report the values of the standard deviation σ_θ as a function of the reduced wind velocity. We observe that the larger the spring stiffness C_{osc} and the moment of inertia J_{osc}, the weaker the amplitude of the oscillations of the flagpole. In Fig. 5(b), we report the relative frequency of oscillation of the flagpole as a function of the reduced wind velocity. It confirms a reduction of the frequency lock-in extension when the stiffness C_{osc} and the moment of inertia J_{osc} are increased while keeping f_{osc} constant.

We now vary the moment of inertia of the oscillator J_{osc} (while keeping C_{osc} constant), and the flag length is adjusted in order to remain at the threshold of flutter instability (i.e. $f_{osc} \simeq f_c^{clamped}$). The corresponding parameters are reported in Table 1. In Fig. 5(c), we report σ_θ as a function of the reduced wind velocity. During each experiment, we observe a regular increase of σ_θ up to a maximum, followed first by a slow decrease and then by a very sharp decrease. In Fig. 5(d), we report the dominant frequency of oscillation of the flagpole and we note that the maximum σ_θ is obtained when the frequency of oscillation of the flagpole is close to the natural frequency of the oscillator. We also observe that the frequency of oscillation of the flagpole converges towards f_{osc} by lower values, and then displays a jump, which marks the end of the frequency lock-in. Concerning the amplitude of rotation, one can notice that increasing the moment of inertia J_{osc} induces a weaker response of the system. At the same time, the extension of the frequency lock-in does not vary significantly. It is then hard to conclude here on the direct impact of J_{osc} on the strength of the coupling. Indeed, in Fig. 5(c,d), an increase of J_{osc} is associated with an increase of the length of the flag and a decrease of the critical flutter velocity.

We now do the same type of experiment by varying the stiffness of the springs and the length of the flag, while all other

Table 1
Characteristics of the set-ups analysed in Fig. 5. In all these experiments, the flag width is fixed $H=100$ mm, the material of the flag is steel, and the damping ratio $\zeta^*_{osc} = 1.4 \times 10^{-2}$ is conserved (relative standard deviation ~10% over more than 30 measurements). In this table, C_{osc} and J_{osc} are respectively the stiffness and the moment of inertia of the oscillator, f_{osc} is the natural frequency of the oscillator, $(f_{osc} - f_c^{clamped})/f_c^{clamped}$ characterized the proximity between the threshold of flutter instability and the frequency lock-in (this parameter has been chosen close to zero in order to trigger the frequency lock-in at low wind velocities), L is the length of the flag, d is the thickness of the flag, E is the modulus of elasticity of the flag (measured with vibrations of a cantilever beam), ρ_s is the mass density of the flag and σ_θ^{max} is the maximal standard deviation of the angle of rotation of the oscillator attached to the flagpole (multiplication of this value by $2\sqrt{2}$ indicates approximately the peak-to-peak amplitude). For comparison purposes, we also indicate the value of the mass parameter M^* of the flags as defined by Eloy et al. (2007).

Set-up	C_{osc} (N m rad^{-1})	J_{osc}(kg m^2)	f_{osc} (Hz)	$\frac{f_{osc} - f_c^{clamped}}{f_c^{clamped}}$	L (mm)	d (μm)	E (N m^{-2})	ρ_s (kg m^{-3})	M^*	$\tilde{B}$ ($\times 10^{-3}$)	σ_θ^{max} (°)
1	0.28	1.0×10^{-4}	8.4	2%	150	54	1.1×10^{11}	7290	0.46	3.4	11.2
2	0.32	1.1×10^{-4}	8.4	2%	150	54	1.1×10^{11}	7290	0.46	3.0	9.4
3	0.62	2.2×10^{-4}	8.4	2%	150	54	1.1×10^{11}	7290	0.46	1.6	10.7
4	0.81	2.9×10^{-4}	8.4	2%	150	54	1.1×10^{11}	7290	0.46	1.2	7.5
5	2.3	8.4×10^{-4}	8.4	2%	150	54	1.1×10^{11}	7290	0.46	4.2	2.9
6	0.32	3.1×10^{-4}	5.0	2%	190	54	1.1×10^{11}	7290	0.58	2.4	6.6
7	0.32	1.8×10^{-4}	6.4	3%	170	54	1.1×10^{11}	7290	0.52	2.7	10.0
8	0.32	1.1×10^{-4}	8.5	3%	150	54	1.1×10^{11}	7290	0.46	3.0	10.3
9	0.32	9.2×10^{-5}	9.2	2%	141	54	1.1×10^{11}	7290	0.43	3.2	10.9
10	0.28	2.2×10^{-4}	5.9	3%	181	54	1.1×10^{11}	7290	0.55	2.8	10.5
11	0.32	2.2×10^{-4}	6.6	3%	170	54	1.1×10^{11}	7290	0.52	2.7	10.0
12	0.62	2.2×10^{-4}	7.7	3%	153	54	1.1×10^{11}	7290	0.47	1.5	11.3
13	0.81	2.2×10^{-4}	9.3	2%	144	54	1.1×10^{11}	7290	0.43	1.2	6.7
14	0.28	1.0×10^{-4}	8.2	4%	154	54	1.1×10^{11}	7290	0.47	3.3	9.8
15	0.28	1.0×10^{-4}	8.2	5%	205	77	1.3×10^{11}	7260	0.44	8.6	18.8
16	0.28	1.0×10^{-4}	8.2	3%	225	103	1.5×10^{11}	7680	0.34	22	27.0

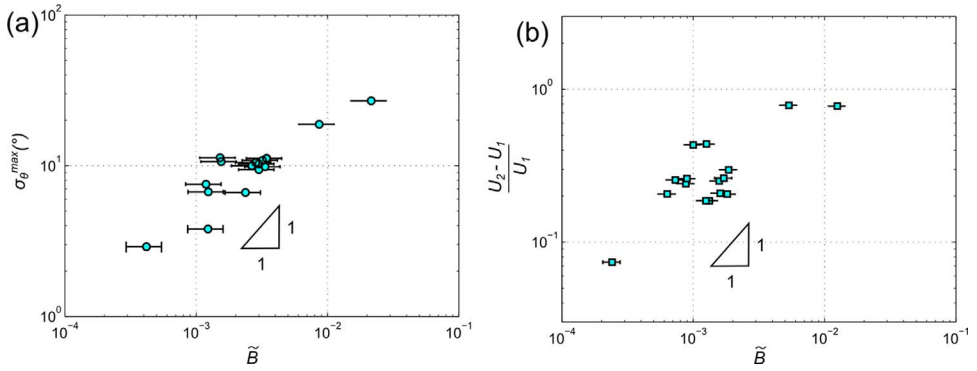

Fig. 6. Coupling between a flag and a spring-mass oscillator as function of the dimensionless rigidity $\tilde{B} = EI/C_{osc}L$ (within two orders of magnitude). The horizontal error bar are the cumulative errors on the estimation of the parameter $\tilde{B}$. (a) Evolution of the maximum standard deviation of the angle of rotation of the flagpole. (b) Evolution of the extension of the frequency lock-in as a function of the dimensionless rigidity $\tilde{B}$.

parameters are conserved, including the proximity with the threshold of instability. The corresponding parameters are reported in Table 1. In Fig. 5(e), we observe that the larger the stiffness of the springs, the weaker the oscillations of the spring-mass oscillator. At the same time, we observe in Fig. 5(f) that the extension of the frequency lock-in is not impacted a lot in this range of parameters.

Finally, we change drastically the bending rigidity of the flag $EI = EHd^3/12$, by changing the thickness of the flag d. The corresponding parameters are reported in Table 1. In Fig. 5(g), we report the values of σ_θ as a function of the wind velocity, for three different thicknesses of steel flags. As before, the length of the flag is adjusted in order to keep the frequency lock-in at the threshold of flutter instability. This leads to a significant modification of the critical flutter velocity as well. The results clearly show that the thicker the flag, the larger the oscillations of the flagpole. Actually, the increase of amplitude for the set-up 16 is so important that the limits of the experimental set-up are fully reached; the springs are non-linearly stretched/compressed and the flag touches the walls of the wind tunnel. Concerning the frequency of oscillation, Fig. 5(h), we observe that the extension of the frequency lock-in also increases as the thickness of the flag increases.

3.2. Discussion

A natural dimensionless number that compares the excitation of the flag to the spring reaction is the ratio of the bending rigidity of the flag to the stiffness of the springs $\tilde{B} = EI/C_{osc}L$ (because the bending moment of the flag $\sim EI/L$ enters in competition with the stiffness C_{osc}). In Fig. 6(a), we report the previous measurements as a function of this dimensionless rigidity $\tilde{B}$. We observe an almost linear evolution between $\log(\sigma_\theta^{max})$ and $\log(\tilde{B})$. In Fig. 6(b), we report the extension of the frequency lock-in as a function of the dimensionless rigidity $\tilde{B}$. The extension of the frequency lock-in is estimated with $(U_2 - U_1)/U_1$, where U_2 is the wind velocity at which the maximum σ_θ^{max} is reached and U_1 corresponds to the wind velocity when σ_θ crosses a conventional value 0.4°. We observe that the extension is also increasing with the dimensionless rigidity $\tilde{B}$.

To conclude, we have reported numerous configurations of coupling by varying the wind velocity, the parameters of flags and the characteristics of the spring-mass oscillators. All the data seemingly depend on a single parameter $\tilde{B} = EI/C_{osc}L$ (see also Virot, 2015, for an alternative model). An interesting parallel can then be made with results obtained in the context of vortex induced vibrations, where the whole dynamics is generally characterized by the Skop–Griffin parameter, which can be seen as a dimensionless rigidity multiplied by the damping ratio (Skop and Griffin, 1973; Khalak and Williamson, 1999; Williamson and Govardhan, 2004). Further investigations would be needed about this parallel, in particular in the context of energy harvesting for which the damping ratio would be a key parameter. It would also be interesting to highlight the coupling between the flagpole motion and the dynamics of the flag. Indeed, as for the case of VIV, it seems that the system can benefit a favorable retroaction of the flagpole on the dynamics of the flag, leading to strong amplitude of oscillation in the lock-in region. The effect of the fluid-solid mass ratio would also be interesting to investigate by carrying the same kind of experiments in water.

The work presented in this paper has been supported by the EDX-DGA program. We thank Ali Bozetine and William Gilbert for very helpful suggestions about the experimental set-up. We acknowledge the DRIP department at École Polytechnique for their encouragements about this work.

References

Akcabay, D.T., Young, Y.L., 2012. Hydroelastic response and energy harvesting potential of flexible piezoelectric beams in viscous flow. Phys. Fluids 24, 054106.
Allen, J.J., Smits, A.J., 2001. Energy harvesting eel. J. Fluids Struct. 15, 629–640.

Ashby, M.F., 2000. Choix des matériaux en conception mécanique, Dunod.
Bae, L., Lee, J., Kim, S., Ha, J., Lee, B.-S., Park, Y., Choong, C., Kim, J.-B., Wang, Z.L., Kim, H.-Y., Park, J.-J., Chung, U.-I., 2014. Flutter-driven triboelectrification for harvesting wind energy. Nat. Commun. 5, 4929.
Bernitsas, M.M., Raghavan, K., Ben-Simon, Y., Garcia, E.M.H., 2008. VIVACE: a new concept in generation of clean and renewable energy from fluid flow. J. Offshore Mech. Arctic Eng. 130, 041101.
Doaré, O., Michelin, S., 2011. Piezoelectric coupling in energy-harvesting fluttering flexible plates: linear stability analysis and conversion efficiency. J. Fluids Struct. 27, 1357–1375.
Dunnmon, J.A., Stanton, S.C., Mann, B.P., Dowell, E.H., 2011. Power extraction from aeroelastic limit cycle oscillations. J. Fluids Struct. 27, 1182–1198.
Eloy, C., Souilliez, C., Schouveiler, L., 2007. Flutter of a rectangular plate. J. Fluids Struct. 23, 904–919.
Giacomello, A., Porfiri, M., 2011. Underwater energy harvesting from a heavy flag hosting ionic polymer metal composites. J. Appl. Phys. 109, 084903.
Gibbs, S.C., Wang, I., Dowell, E., 2012. Theory and experiment for flutter of a rectangular plate with a fixed leading edge in three-dimensional axial flow. J. Fluids Struct. 34, 68–83.
Howell, R.M., Lucey, A.D., 2014. Stability of a spring-mounted cantileverd flexible plate in a uniform flow. In: Zhou, Y., Liu, Y., Huang, L., Hodges, D.H. (Eds.), Fluid–Structure–Sound Interactions and Control, Springer, Springer-Verlag, Berlin, Heidelberg, pp. 319–329.
Jia, L., et al., 2015. Response of a flexible filament in a flowing soap film subject to a forced vibration. Phys. Fluids 27, 017101.
Khalak, A., Williamson, C.H.K., 1999. Motions, forces and mode transitions in vortex-induced-vibrations at low mass-damping. J. Fluids Struct. 13, 813–851.
Landau, L.D., Lifshitz, E.M., 1976. Mechanics, third edition. Butterworth Heinemann, Oxford.
Michelin, S., Doaré, O., 2013. Energy harvesting efficiency of piezoelectric flags in axial flows. J. Fluid Mech. 714, 489–504.
Singh, K., Michelin, S., deLangre, E., 2012. The effect of non uniform damping on flutter in axial flow and energy harvesting strategies. Proceedings of the Royal Society A 468, 3620–3635.
Skop, R.A., Griffin, O.M., 1973. An heuristic model for determining flow-induced vibrations of offshore structures. In: 5th Offshore Technology Conference OTC-1843-MS, 1973.
Stone, B.N., Lucey, A.D., Howell, R.M., 2013. The fluid–structure interaction of a torsional-spring-mounted beam in air flow. In: 2nd Book of Extended Abstracts, Department of Mechanical Engineering, Curtin University, Australia: pp. 103–104.
Tang, L., Païdoussis, M.P., Jiang, J., 2009. Cantilevered flexible plates in axial flow: energy transfer and the concept of flutter-mill. J. Sound Vib. 326, 263–276.
Taylor, G.W., Burns, J.R., Kammann, S.M., Power, W.B., Welsh, T.R., 2001. The energy harvesting eel, a small subsurface ocean-river power generator. J. Ocean. Eng. 26, 539–547.
Virot, E., Amandolese, X., Hémon, P., 2013. Fluttering flag: an experimental study of fluid forces. J. Fluids Struct. 43, 385–401.
Virot, E., 2015. Flottement de drapeau: dynamique et couplage (Ph.D. Thesis), École Polytechnique (in French).
Williamson, C.H.K., Govardhan, R., 2004. Vortex-induced vibrations. Ann. Rev. Fluid Mech. 36, 413–455.
Xia, Y., Michelin, S., Doaré, O., 2015. Fluid–solid–electric lock-in of energy-harvesting piezoelectric flags. Phys. Rev. Appl. 3, 014009.